RESEARCH ARTICLE

Neural Network Based Predictive Current Controllers for Three Phase Inverter

SÜLEYMAN YARIKKAYA[1] **AND KADİR VARDAR**[2], **(Member, IEEE)**
[1]Dinar Vocational School, Computer Programming, Afyon Kocatepe University, 03200 Afyonkarahisar, Turkey
[2]Electrical and Electronics Engineering Department, Kütahya Dumlupınar University, 43100 Kütahya, Turkey

Corresponding author: Kadir Vardar (kadir.vardar@dpu.edu.tr)

ABSTRACT With Predictive Current Controllers, system behavior or current reference is predicted. In this way, it is aimed to prevent hardware and software related delays. In this study, new Artificial Neural Network (ANN) based Predictive Current Controllers are designed using four different methods for voltage source inverters. The training of the networks is done offline using the data obtained from the simulation results for different parameters in the Matlab environment. In the first proposed method, a static ANN based current controller is designed and trained using the data obtained from the Finite Control Set Model Predictive Control (FCS-MPC) method. Then, a feed-forward reference current predictor ANN (PRefNN) is designed to make sinusoidal reference current prediction in the other three methods. The other proposed predictive ANN methods are trained by taking the data offline from the inverter system in which PRefNN and the classical current controllers (Hysteresis, PR, and PI) are used. In this way, three different predictive current controllers named as Hysteresis based predictive ANN (Hist-PNN), PR based predictive ANN (PR-PNN), and PI based predictive ANN (PI-PNN) are designed. Classical current control methods have been given predictive properties with these three different network structures. And also, it is improved the performance of classical methods against parameter changes and noises. A three phase 5kVA inverter circuit with a 7MBP50RJ120 IPM module in the power stage and STM32f407 as a controller is designed for the experimental setup. The methods are tested in simulation and validated in the experimental setup.

INDEX TERMS Artificial neural networks, current controller, model predictive control, predictive current controller, three phase inverters.

I. INTRODUCTION

Artificial Neural Network (ANN) is one of the popular control methods used recently. It is an approximation model used for systems where the model is unknown or nonlinear. Thanks to its function approximation capability, it is useful for controlling nonlinear, discrete-time, and complex systems [1], [2]. ANN-based controllers and estimators are widely used in the identification and control of power converters and motor drives [3], [4]. ANN generally improves the performance of the system. It can be designed with previously obtained data without needing a system or facility model. It can also reduce high hardware and software requirements in some cases [4], [5]. Model Predictive Control (MPC) is an accepted control strategy in both academic research and industrial applications. Academic studies on MPC have increased significantly in recent years [6], [7], [8], [9]. Especially with the contribution of the developments in control elements, the use of MPC in converters and drivers in power electronics has become an attractive solution [8], [9], [10]. MPC is relatively easy to implement in multivariate systems and offers a fast dynamic response. It also allows nonlinear systems and constraints to be conveniently incorporated into the controller. It has several advantages, such as combining multiple control parameters in one loop [10], [11]. The disadvantages are modelling difficulties, sensitivity to load parameter variation and high computational burden [12], [13], [14].

MPC uses the system model to predict the future value of the controlled variables. According to the optimization equation created, these estimated values are used to obtain the desired optimal activation. MPC techniques used in

The associate editor coordinating the review of this manuscript and approving it for publication was Sze Sing Lee.

Power Electronics are classified into two main categories: Continuous Control Set MPC (CCS-MPC) and Finite Control Set MPC (FCS-MPC). CCS-MPC uses a modulator that produces output with a fixed switching frequency. FCS-MPC generates the switching signals directly, and no modulator is needed. It uses a limited number of possible switching states for optimization. System behavior is predicted for all switching positions using a discrete model. The most appropriate switching position is determined and applied by evaluating these estimates in a weighting function. The main advantage of FCS-MPC is that it is used directly to the converter without a modulation stage [10], [15], [16].

In a conventional MPC controller, the mathematical model parameters of a variable load system need to be controlled during operation. System efficiency decreases as the weighting function must also be evaluated online at each sampling interval. Therefore, the optimal control law is obtained under various load conditions by applying the MPC based ANN (MPC-ANN) control method with offline training [17]. The high horizon length in the FCS-MPC method increases the algorithm's complexity. Since the data from the FCS-MPC method is used to train the system using the MPC-ANN method, a similar prediction horizon length is obtained. However, there is no additional complexity in the computational burden of the MPC-ANN structure.

There are various studies in which MPC and ANN are used together. These studies are on controlling a system parameter or the whole system. In the study with reference [18], the weighting function parameters used in FCS-MPC (λ_{DC} and λ_{SW}, DC bus balance and switching frequency, respectively) are produced from an ANN output trained for this task and controlled. In another study given by [19], PI control parameters are continuously adjusted using a predictive neural network controller (PNNC) in a grid-connected PV inverter controller. The PNNC estimates the control parameters by monitoring the errors of the grid currents and the DC-bus voltage. In [20], an MPC based neural network controller is proposed for a three-phase four-level flying capacitor inverter. Offline MPC simulation data were obtained, and ANN was trained using these data. Two studies that take advantage of the flexibility of MPC at training time in [4] and [17] propose a feed-forward ANN based controller for a three-phase inverter with output LC filter for UPS applications. It is aimed to achieve lower THD and improve dynamic performance for different load types. ANN is trained offline using the data from the simulation results of FCS-MPC. Filter current(i_f), output current(i_0), output voltage (V_C), and output reference voltage (V_{C*}) are used as ANN input. Voltage vector (Xopt) is obtained from ANN output, and inverter output voltage control is performed. In [21], an algorithm with less computational burden is obtained by training the ANN from the FS-MPC algorithm in a UPS application. In [22] and [23], firstly, the simulation of a grid connected VSC system, including CCS-MPC and classical PI controllers was carried out for training data collection.

In training the designed PI-based ANN and MPC-based ANN networks, the data were obtained by simulation in a Matlab environment and the supervisor learning technique was used.

Inverters are usually digitally controlled, so software and hardware delays occur. These delays affect the performance of the inverters. In particular, the output frequency characteristics of inverters are affected, and phase shifts may occur, making them unstable. Predictive approaches can be used to compensate for these delays [24], [25].

This study aims to design Predictive based ANN current controllers to control the inverter output current. As a result of the studies carried out using 4 different methods, 4 different Predictive based ANN current controllers are designed and presented. In the first proposed method, ANN was trained offline using the data obtained from the FCS-MPC simulation and used as current controller (CC) in the inverter. Unlike those in the literature, the input of the network is the current reference iref(k), the current error ie(k) and the previous value of the current error ie(k-1), the output of the network is the switching states.

A feed-forward ANN reference current predictor (PRefNN) network has been designed to make sinusoidal reference current prediction in the other three methods. With this block, it is aimed to generate the reference current iref(k+2) value belonging to the next two sampling time steps. In the design phase of the second Predictive ANN CC structure realized, the training data is taken off-line from the simulation, where Hysteresis CC follows the predicted reference inverter current generated with PRefNN. Using these data, a feedforward static ANN block with 3 neurons in the hidden layer was created. The inputs of the designed Hysteresis-based Predictive ANN (Hist-PNN) current controller are a reference and actual currents in the abc-axes. The network outputs are the switching states (S_a, S_b, S_c). In the third method, the training data for the network training was obtained from the simulation using the PRefNN reference current predictor and the Proportional Resonant (PR) current controller. The proposed PR based Predictive ANN (PR-PNN) current controller consists of a dynamic feed-forward ANN with 2 neurons in the hidden layer. The PR-PNN inputs are the current error, the previous value of the current error, and the previous value of the output in the $\alpha\beta$-axes. The network's output is the inverter reference voltages in the $\alpha\beta$-axes. Similarly, training data was obtained from a system containing PRefNN and PI current controllers in the fourth ANN-based predictive current controller. The inputs of the trained PI-based predictive ANN (PI-PNN) network are the inverter reference currents in the dq-axes and the previous value of the network's output. Its output is the inverter reference voltages in the dq-axes. PI-PNN is a dynamic feed-forward network structure with 2 neurons in the hidden layer.

A three-phase 5 kVA inverter circuit was designed in a laboratory environment for the experimental work. The control card was created using the STM32f407
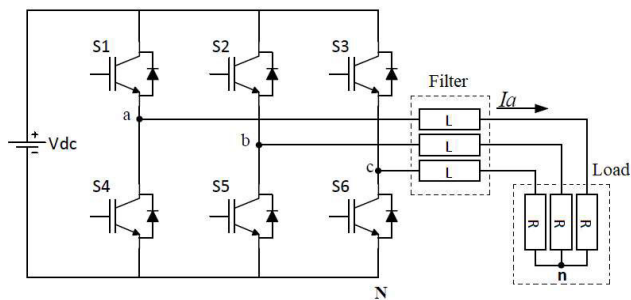
FIGURE 1. Three-phase VSI inverter structure.

FIGURE 2. Voltage vector representation of eight possible switching states and all switching states.

microcontroller. The inverter control software was prepared using MikroC language for the 4 different methods designed, and experimental verification was carried out by loading them into the inverter system.

Section II presents the voltage source inverter (VSI) structure used in the study and the mathematical model of FCS-MPC created for this inverter structure. In Section III, the proposed and designed predictive ANN models are explained in detail and compared structurally. The obtained simulation and experimental application results are given in Section IV. The conclusions obtained are presented in Section V.

II. THREE PHASE INVERTER STRUCTURE AND FCS-MODEL PREDICTIVE CONTROLLER

A. TWO LEVEL VOLTAGE SOURCE INVERTER TOPOLOGY

In this study, a two-level VSI is used, which is the most preferred DC/AC converter in industrial applications. In addition, it has a structure and working principle that can be easily extended to other topologies. The three-phase two-level VSI structure is shown in Fig.1. For each phase output, there is a phase leg and two switches that provide positive (P) and negative (N) busbar connections. These two switches work as complements of each other to avoid short circuits in DC source. There is a desired state for the control of each phase leg, and two switches are controlled according to this situation [15], [26], [27]. A total of 6 semiconductor switches (S1, S2, S3, S4, S5 and S6) are controlled as three states (S_a, S_b, and S_c) and their complements (S_a', S_b', and S_c').

B. FINITE CONTROL SET -MODEL PREDICTIVE CONTROLLER (FCS-MPC)

FCS-MPC is preferred because it is simpler than other MPC in terms of ease of understanding and implementation. FCS-MPC is an MPC method that emerged in power electronics with its discrete structure. FCS-MPC does not require a modulator due to its structure and switching positions are produced directly after calculations. A state output selection is made for controlling semiconductors. These are one of the 8 possible switching states for DC/AC inverter control with 3 main control signals (Sa, Sb, Sc).
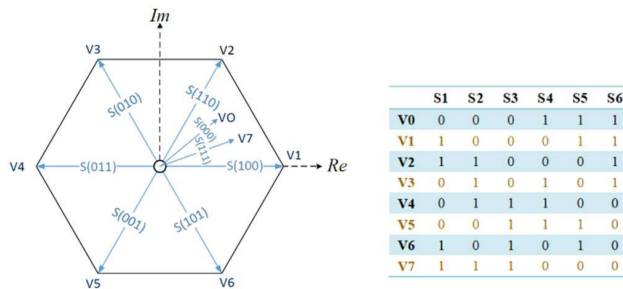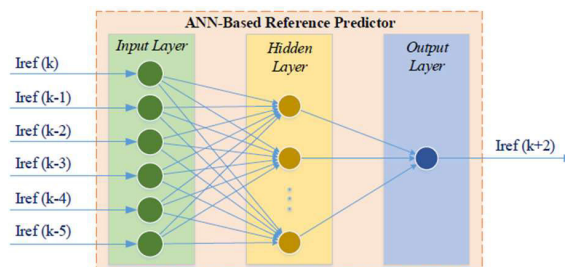

FIGURE 3. Network structure of the PRefNN block.

When only one voltage vector (Fig.2) is used for each control period, the drive output ripple is large. Also, when FCS-MPC is used at the variable switching frequency, filter design becomes more complex as output voltage and current harmonics spread over a wide frequency range. The fixed frequency output is recommended to reduce output harmonics [8], [28], [29].

According to Fig.1, if the inverter output voltages are written as Vdc based on the N point, the following (1) is obtained.

$$\begin{bmatrix} U_{aN} \\ U_{bN} \\ U_{cN} \end{bmatrix} = \begin{bmatrix} S_a \\ S_b \\ S_c \end{bmatrix} * V_{dc} \qquad (1)$$

where, Vdc is the DC-link voltage, and U_{aN}, U_{bN}, and U_{cN} are the inverter output voltages. According to Fig.1, when the branch currents are followed, the following equations are obtained when KVL is applied.

$$\begin{cases} L\dfrac{di_a}{dt} = U_{an} - Ri_a \\ L\dfrac{di_b}{dt} = U_{bn} - Ri_b \\ L\dfrac{di_c}{dt} = U_{cn} - Ri_c \end{cases} \qquad (2)$$

where, L is the filter inductance, R is the load resistance, i_a, i_b, and i_c are the inverter output currents.

$$\frac{di_x}{dt} = \frac{i_x(k+1) - i_x(k)}{T_S} \qquad (3)$$

If we substitute the Forward Euler method equation given in (3) for each phase in (2), (4) is obtained.

$$\begin{cases} i_a\,(k+1) = \dfrac{T_s}{L}\,[U_{an}\,(k) - Ri_a\,(k)] + i_a\,(k) \\[2mm] i_b\,(k+1) = \dfrac{T_s}{L}\,[U_{bn}\,(k) - Ri_b\,(k)] + i_b\,(k) \\[2mm] i_c\,(k+1) = \dfrac{T_s}{L}\,[U_{cn}\,(k) - Ri_c(k)] + i_c(k) \end{cases} \quad (4)$$

The above equations are obtained for the abc-axes. These equations are converted to $\alpha\beta$-axes with the help of Clarke transform and the inverter model equation given by (5) is obtained [28].

$$\begin{cases} i_\alpha\,(k+1) = \dfrac{T_s}{L}\,[U_{\alpha n}\,(k) - Ri_\alpha\,(k)] + i_\alpha\,(k) \\[2mm] i_\beta\,(k+1) = \dfrac{T_s}{L}\,\left[U_{\beta n}\,(k) - Ri_\beta\,(k)\right] + i_\beta\,(k) \end{cases} \quad (5)$$

Here, i_α and i_β are the real and imaginary values of the inverter output currents, Ts is the sampling time.

The weighting function is used for the optimization stage. Using the weighting function in (6), valid values for all subsequent possible switching states are obtained. As a result of these functions, the switching state with the lowest g value is selected. Weighting function [30] for VSI current control:

$$g = \left| I_\alpha^* - I_\alpha^p \right| + \left| I_\beta^* - I_\beta^p \right| \quad (6)$$

Here, $I_\alpha^p = i_\alpha(k+1)$ and $I_\beta^p = i_\beta(k+1)$ are obtained from (5). I_α^* and I_β^* are inverter current references. With this structure, the three-phase inverter output current is controlled by predicting a one-step prediction horizon.

III. PROPOSED PREDICTIVE ANN CONTROLLERS

In this study, four different ANN-based current controller models with predictive features are proposed. In the first model, ANN was trained using the data obtained from the MPC structure and used as a current controller (MPC-ANN). To make sinusoidal reference current prediction, which is common to the other three methods, a current reference predictive ANN network (PRefNN) has been designed.

PRefNN generates the reference current iref(k+2) information belonging two sampling time steps later. In the second Predictive ANN CC (Hist-PNN) method implemented, the simulation in which the reference inverter current is generated with PRefNN, and this reference current is followed using the Hysteresis current controller, was used to collect the training data offline. Similarly, In the third method, PRefNN and PR current controller were used, and in the fourth method, PRefNN and PI current controller was used to obtain training data, and network designs were carried out (PR-PNN and PI-PNN). Reference generator PRefNN and designed four different ANN-based current controller models are presented below.

A. ANN-BASED SINUSOIDAL REFERENCE CURRENT PREDICTOR (PREFNN)

In the design phase, a structure was needed to estimate the two sampling time steps later value of a sinusoidal signal. Thus, the next values of the generated reference currents (abc or $\alpha\beta$) can be predicted. The data were taken over the unit sine signal in the training phase. The input data are the unit sine signals current and past five samples. The output is determined as the value of the unit sine two sampling times after the current sample. This way, data were obtained by shifting the sampling time, and a feedforward ANN structure was trained with these data. The created reference predictive neural network (PRefNN) structure has six inputs, one hidden layer, and one output. The hidden layer consists of ten neurons and the hyperbolic tangent sigmoid (tansig) activation function. The output layer consists of a neuron and a pure-line activation function. Levenberg-Marquardt backpropagation method was used in PRefNN training. Fig.3 shows the network structure, inputs, and outputs of PRefNN.

The sampling time in the training was determined as 50 μs. Using this block, Iref(k+2) will be obtained by predicting two sampling time steps after the reference current value (100 μs). It can be used for a single phase. The required number should be added for each phase (abc or $\alpha\beta$).

B. MODEL-1: MPC BASED ANN CURRENT CONTROLLER (MPC-ANN)

Firstly, an MPC-based ANN (MPC-ANN) current controller is proposed to control the inverter output current. For training the MPC-ANN current controller, an inverter simulation using FCS-MPC as the current controller is created in the Matlab/Simulink simulation environment. In the inverter simulation, there are eight different switching states for the output of FCS-MPC. For these cases, using the discrete-time model in (5), the inverter output current for one step ahead is predicted. In the weighting function in (6) evaluates these predicted current values, and the best switching states are selected. Using this switching state information, all switching signals are generated and applied to the inverter switches during a sample time of Ts. Since the load parameter (L and R) values are entered as model constants in FCS-MPC, the inverter operates at a constant load. To operate at different loads, the load constants used in the model need to be changed. The inverter simulation was run by adjusting the parameters for different load conditions, and the training data were obtained offline separately. The collected training data consists of 2400 data series for each input or output variable. The scaled Conjugate Gradient Backpropagation method was used to train the MPC-ANN current controller. The training was completed after 81 iterations, and as a result of the training, the cross entropy (CE) was 0.065829, and the error output rate (E) was 18.98809.

The network created for MPC-ANN is a feed-forward static network structure with six inputs, one hidden layer, and seven outputs (Fig.5). The inputs of the network are the
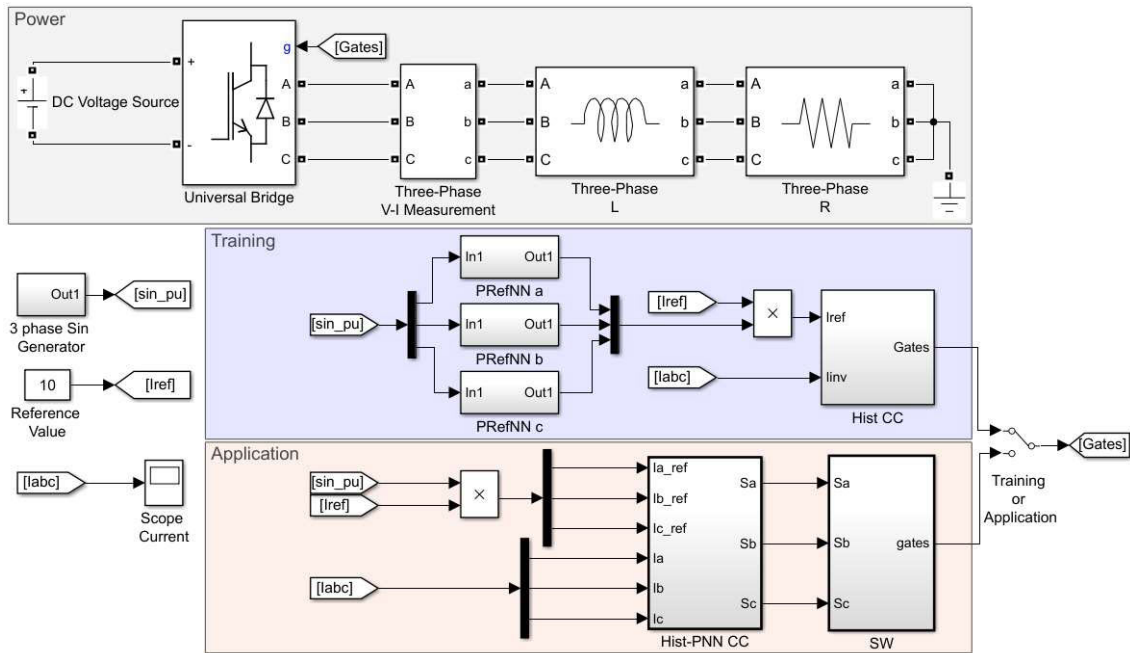
FIGURE 4. Block diagram of the simulation of VSI used to train and run the Hist-PNN current controller.
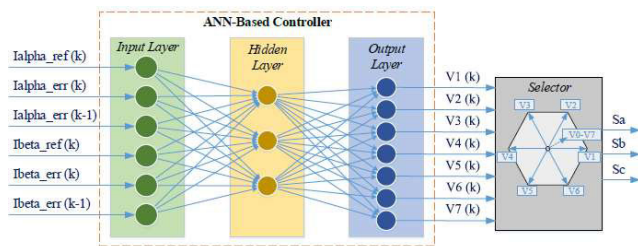

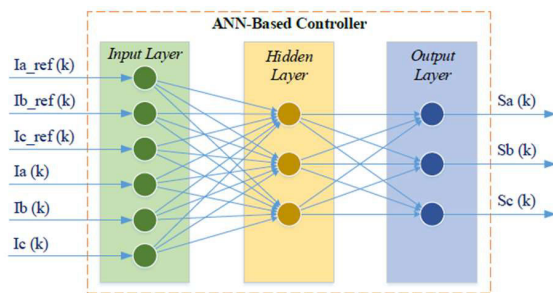**FIGURE 5.** Network structure of MPC-ANN current controller.

FIGURE 6. Network structure of Hist-PNN current controller.

reference current Iref(k), the current error Ierr(k), and the previous value of the current error Ierr(k-1) in the $\alpha\beta$ axes. Three neurons are in the hidden layer, and the sigmoid is used as the activation function. Each of the network outputs represents a switching position in the space vector. The softmax function is used as the output activation function.

The proposed MPC-ANN current controller takes the input values at every k sampling time and calculates the outputs

using these values in the ANN structure. The outputs of the MPC-ANN are obtained as values representing seven possible positions of the space vector. At any sampling step, only one of these seven outputs produces output one, and the others output zero. The output with a value of one is the index value of the space vector to be generated. For this index value, switching states information is obtained from the space vector, and switching functions (Sa, Sb, Sc) are generated.

C. MODEL-2: HYSTERESIS BASED PREDICTIVE ANN CURRENT CONTROLLER (HIST-PNN)

In the second proposed model, a reference predictive hysteresis-based ANN (Hist-PNN) is designed that controls the inverter output current by predicting two sampling time steps ahead of the reference current (100 μs). First, an inverter simulation was prepared using PRefNN and Hysteresis CC, which predict two steps ahead of the reference current value in Section III-A, to obtain training data from the Matlab/Simulink environment. The simulation block diagram used for training and testing is given in Fig.4. Since the Hysteresis CC works in abc coordinate axes, a separate PRefNN block is used for each phase. Obtained reference currents (k+2)th values were followed by Hysteresis CC, and of the network are the reference current and inverter currents inverter switching information was produced. The input data of the network are the reference current and inverter currents in the abc coordinate axes. Its output is the switching signals of each phase. ANN structure and input and output information are shown in Fig.6.

In the simulation, the hysteresis band is 0.1 A, the control algorithm operating frequency is 20 kHz, filter inductance
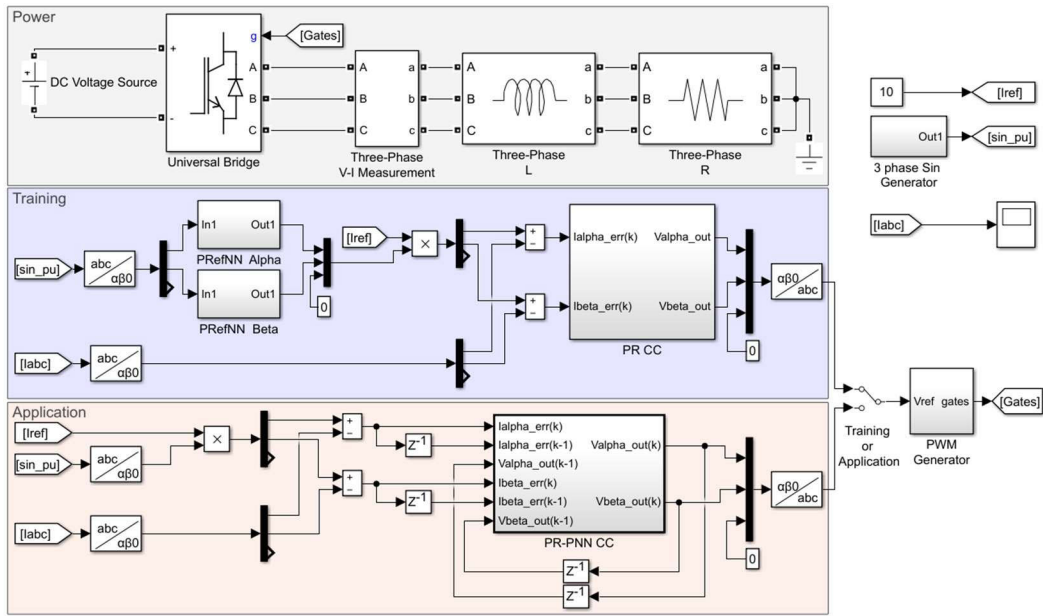
FIGURE 7. Block diagram of the simulation of VSI used to train and run the PR-PNN current controller.

is 3mH and the simulation run step time is 1 μs. Training data were obtained using 3A, 6A, and 8A reference currents values. For each input-output, 1200 data series were obtained offline. The Hist-PNN current controller is designed as a feedforward static network structure and is trained with these data. Levenberg-Marquardt backpropagation method was used in training. The training was completed with a Mean Square Error (MSE) of 0.0214966 and a regression value of 0.95604. Hist-PNN is a network consisting of six inputs, three outputs, and one hidden layer. The hidden layer consists of three neurons, and the tansig activation function is used. In the output layer, the pure-line function is used.

The Matlab/Simulink block diagram used for obtaining training data and testing the designed network is given in,Fig.4. In the application phase, simulation tests were performed at different reference current values, and the network was verified.

D. MODEL-3: PR BASED PREDICTIVE ANN CURRENT CONTROLLER (PR-PNN)

In this model, a reference predictive PR-based ANN (PR-PNN) is designed, which controls the inverter output current by predicting two sampling time steps ahead (100 μs) of the reference current. First, an inverter simulation, including PRefNN, which predicts the two sampling time steps ahead of the reference current, and PR CC, was prepared to obtain training data in Matlab/Simulink environment. The simulation block diagram used for training and testing is given in Fig.7. Since the training takes place in the α and β coordinate axes, two PRefNN blocks were used. The $(k+2)$th values of the generated $\alpha\beta$ reference currents were followed by two PR CCs and inverter reference voltage
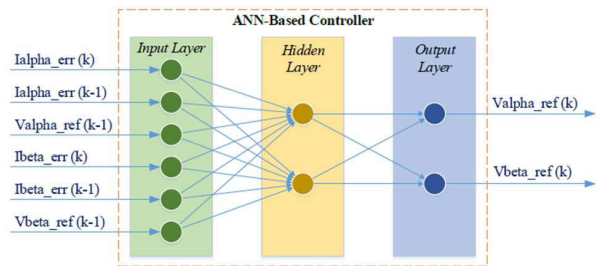

FIGURE 8. Network structure of PR-PNN current controller.

information was created. In the simulation, PR CC outputs references voltage in the $\alpha\beta$-axes are converted to the abc-axes coordinate. The PWM generator block generates the inverter switching signal by comparing it with the 20kHz triangle signal.

The training data were obtained in the simulation using 3A, 6A, and 8A reference current values for the filter inductance of 3mH. Random noise was added to the received data in order to increase the performance of the network. The training was completed with an MSE of 0.00206879 and a regression value of 0.99999. The training was not possible with ANN structures in the static structure designed using the data obtained with this method. For this reason, different network designs have been studied.

As a result, a dynamic network structure has been developed, including the input-output information seen in Fig.8, and the outputs are also fed back as the network's input. The designed PR-PNN current controller structure consists of six inputs, two outputs, and one hidden layer. There are two neurons in the hidden layer. ANN inputs
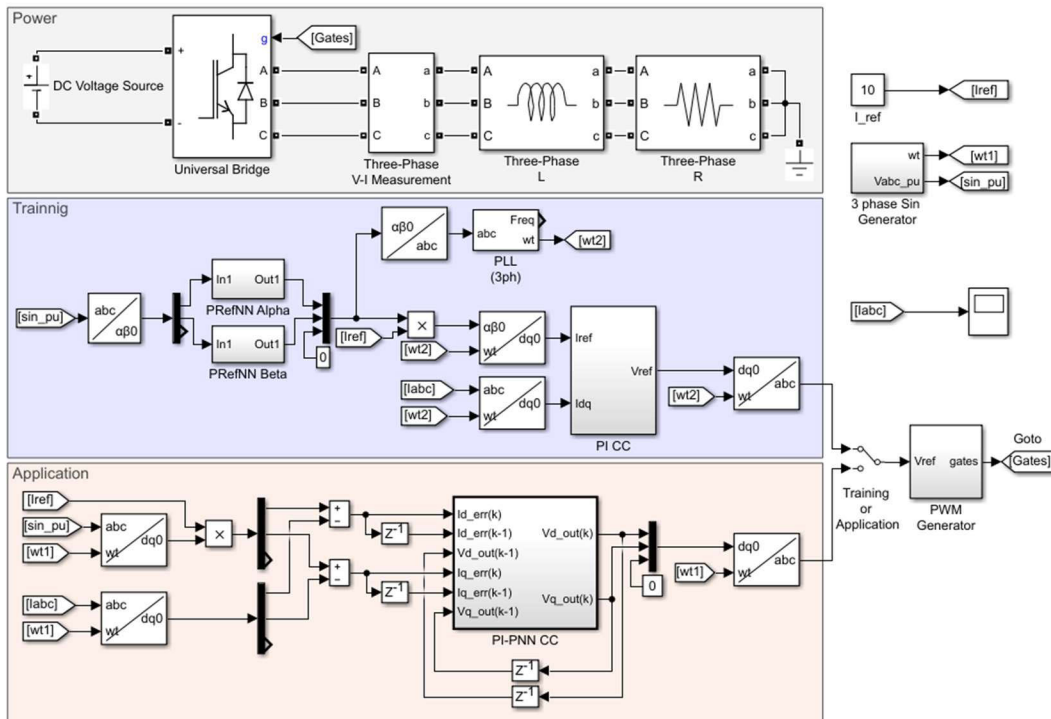
FIGURE 9. Block diagram of the simulation of VSI used to train and run the PI-PNN current controller.

are current errors and previous values of current errors for the $\alpha\beta$-axes [Ialpha_err(k), Ialpha _err(k-1), Ibeta_err(k) and Ibeta_err(k-1)]. In addition, the other two inputs are the previous values of the $\alpha\beta$ reference voltages, which are also outputs [Valpha_ref(k-1) and Vbeta_ref(k-1)]. ANN outputs are reference voltages in the $\alpha\beta$-axes [Valpha_ref(k) and Vbeta_ref(k)]. The pure-line function in the hidden layer and the tansig function in the input layer is used as the activation function. The training was carried out using the Levenberg-Marquardt backpropagation method. Wcut=2.5 and w=314.1593 were used for the PR current controller parameters during the training phase.

In Fig.7, the Matlab/Simulink block diagram is given for receiving training data and testing the designed network. In the application phase, the network was verified by performing simulations for different reference current values.

E. MODEL-4: PI BASED PREDICTIVE ANN CURRENT CONTROLLER (PI-PNN)

The fourth model, a reference predictive PI-based ANN (PI-PNN), is designed to control the inverter output current by predicting two sampling time steps ahead ($100\mu s$) of the reference current. To obtain training data in Matlab/Simulink environment, an inverter simulation including PRefNN and PI CC was prepared. The simulation block diagram used for training and testing is given in Fig.9. While receiving the training data, two PRefNN blocks operating in the α and β coordinate axes were used to predict the reference current. The generated $\alpha\beta$ reference currents (k+2)th values

were then converted to dq coordinate axes. The theta value required for this conversion was generated using the predicted reference currents with the help of a PLL circuit. Two PI CCs followed the generated dq-axes reference currents, and inverter reference voltage information was created. In the simulation, dq-axes references voltage, which are PI CC outputs, are converted to coordinate abc-axes, and the inverter switching signal is produced by comparing the 20kHz sawtooth signal by the PWM generator block.

The training data were collected from the simulation results for the filter inductance of 3mH and the 3A, 8A values of the reference currents. The random noise was added to the received training data in order to increase the performance of the network. The training was completed with an MSE of 0.00177157 and a regression value of 0.99999. Different static ANN structures operating in $\alpha\beta$-axes or dq-axes have been studied but training these structures has not been possible. For this reason, a dynamic neural network structure with input-output variables seen in Fig.10 is designed.

The proposed PI-PNN current controller structure consists of six inputs, two outputs, and one hidden layer. There are two neurons in the hidden layer. ANN inputs are current errors and previous values of current errors for the dq-axes [Id_err(k) Id_err(k-1), Iq_err(k), and Iq_err(k-1)]. The other two inputs are the previous values of the dq-axes reference voltages, which are also the network's output [Vd_ref(k-1) and Vq_ref(k-1)]. ANN outputs are reference voltages in the dq-axes [Vd_ref(k) and Vq_ref(k)]. As the activation function, the pure-line function is used in the hidden layer,

TABLE 1. Comparisons of the tasks and sizes of proposed ANN-CCs.

	Reference Frame ANN inputs	ANN outputs	Number of inputs	Hidden Layer Neurons	Number of outputs	Modulator	Training Algorithm	ANN Transfer Functions
MPC-ANN	alpha-beta	Space vector index-Gate pulses	6	3	7	no	scaled conjugate gradient backpropagation	Tansig/Softmax
Hist-PNN	abc	Gate pulses	6	3	3	no	Levenberg-Marquardt backpropagation	Tansig/Pureline
PR-PNN	alpha-beta	Valpha_ref-Vbeta_ref	6	2	2	PWM	Levenberg-Marquardt backpropagation	Tansig/Pureline
PI-PNN	dq	Vd_ref-Vq_ref	6	2	2	PWM	Levenberg-Marquardt backpropagation	Tansig/Pureline
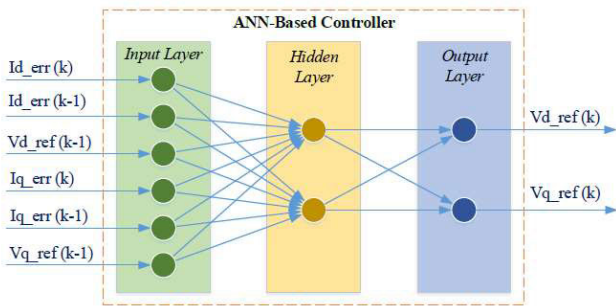
FIGURE 10. Network structure of PI-PNN current controller.

TABLE 2. Parameter of the simulation and experimental setup.

Symbol	SYSTEM PARAMETERS	Values
f	Output frequency	50 Hz
Vdc	DC link voltage	210 V
L	Filter inductance	8 mH
R	Load resistance	10 Ω
Ts	Sampling time	50 μs

and the tansig function is used in the input layer. The training was carried out using the Levenberg-Marquardt backpropagation method.

In Fig.9, the Matlab/Simulink block diagram, which is used for receiving training data and testing the designed network, can be seen. During the application phase, the network was verified by performing simulation tests for different reference current values. The general specifications of the four proposed controllers are given in Table 1.

IV. SIMULATIONS AND EXPERIMENTAL WORKS
A. SIMULATION RESULTS
In this section, simulation and experimental results with different reference current values for four models of predictive ANN current controllers are presented. The parameters of the simulation and experiment system are listed in Table 2.

The results obtained from the simulations of these four different methods shown in Fig.4, Fig.7, and Fig.9 are presented in Fig.11. In simulations, the inverter reference current is determined as 2A up to t=0.03s, 5A between t=0.03s– 0.06s and 10A after t=0.06s. When the simulation results are examined, it is seen that a stable operation is obtained for all methods.

In addition to the simulation results given in Fig.11, harmonic distortions of the inverter current are also noted in classical control structures (FCS-MPC, Hysteresis, PR, and PI CC), where training data is taken for each method. In simulations, the total harmonic distortion (THD) for FCS-MPC CC is 2.35%, and THD for MPC-ANN CC is 2.74%. THD for classical Hysteresis CC is 3.73%, and THD for Hist-PNN CC is 3.37%. In classical PR CC and PR-PNN CC simulations, the THD value is 0.52% for both. Finally, THD 0.54% for classic PI CC and THD 0.51% for PI-PNN CC.

In Fig.12, it is tested and presented whether they show the prediction feature of the methods. For this purpose, the phase currents obtained from the inverter output for the classical Hysteresis and Hist-PNN current controllers are plotted on the same graph and presented in Fig.12.a. The graph shows that the inverter current zero volts (0V) transition is at 0.0899s for Hist-PNN and at 0.09s for classical Hysteresis CC. This indicates the ability to predict the intended 100μs ahead before the training is acquired. Similarly, in Fig12.b, it is seen that the phase current produced at the inverter output using the PR- PNN current controller is 100μs ahead of the current produced at the inverter output using the PR current controller. In Fig.12.c, the inverter output current controlled by PI-PNN is 100μs ahead of the inverter output current controlled by PI CC. The results of the FCS-MPC and MPC-ANN methods are not given since both methods have predictive properties. According to the results obtained in Fig.12, it has been observed that all methods can predict successfully.

To understand the controller performances, the control surface graphs of the methods are presented in Fig.13. Control surface graphs could not be obtained for the MPC-ANN
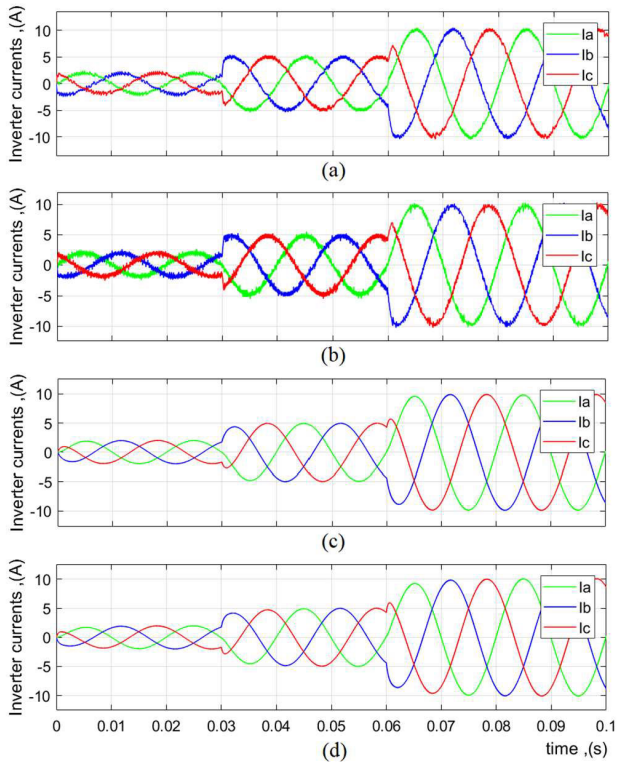
FIGURE 11. Simulation results of VSI; the inverter output currents for (a) MPC-ANN, (b) His-PNN, (c) PR-PNN, and (d) PI-PNN.
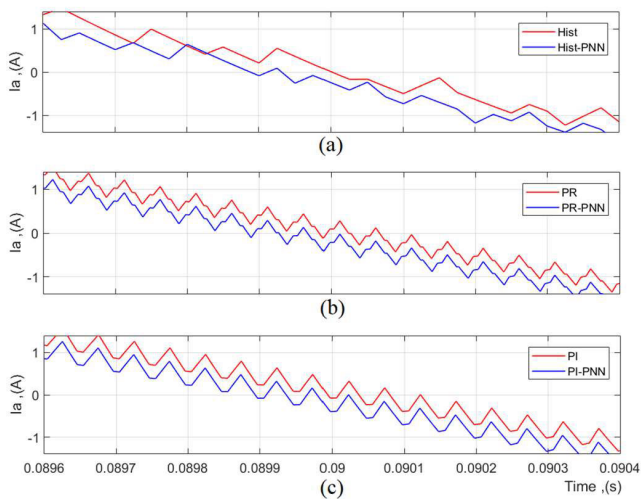

FIGURE 12. Time difference graph of output currents (a) Histerisis and Hist-PNN, (b) PR and PR-PNN, (c) PI and PI-PNN.
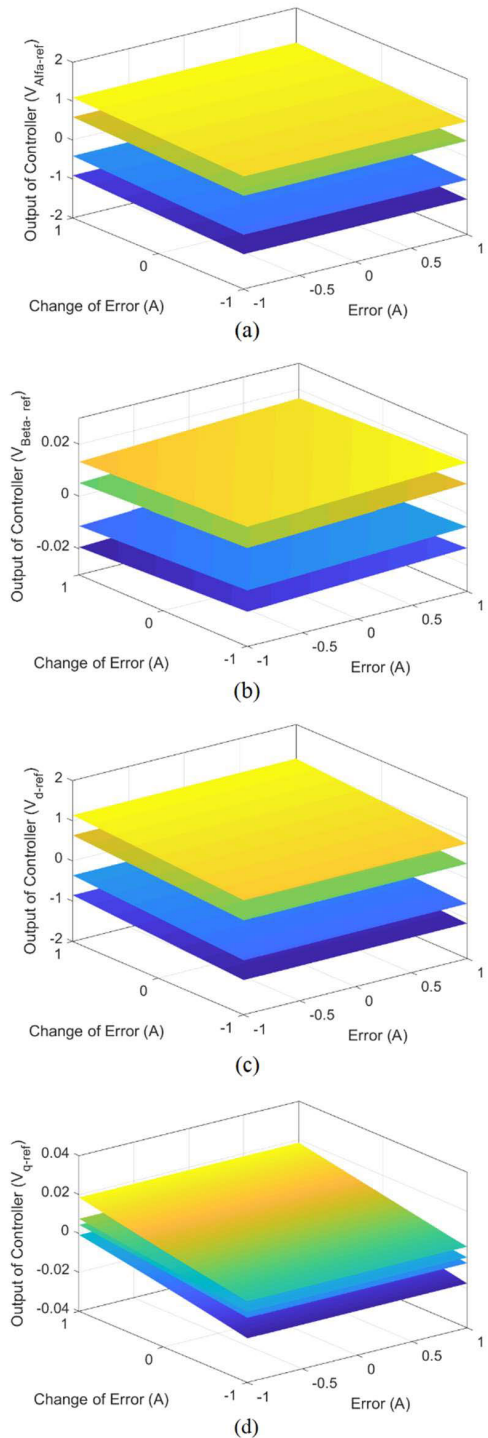

FIGURE 13. Surface graphs of controllers for (a) α-axis output of PR-PNN, (b) β-axis output of PR-PNN, (c) d-axis output of PI-PNN, and (d) q-axis output of PI-PNN.

and Hist-PNN methods since the output is direct switching signals. For other methods, since the number of network entries is high, some of them were kept constant, and the results were recorded according to the changes of others. The surface graphs for the α-axis and β-axis voltage reference outputs of the PR-PNN method are presented in Fig.13a and 13b. PR- PNN has six inputs, and the inputs in the β-axes [(Ibeta_err(k), Ibeta_err(k-1) and Vbeta_ref(k-1)]

are taken as zero when plotting the Valpha_ref output graph. The other inputs, the α-axis current error and its previous value [alpha_err(k), Ialpha_err(k-1)], were changed in the range of ± 1 A. For the third entry, Valpha_ref(k-1), four different surface graphs were obtained using constant values of -1, -0.5, +0.5, and +1 (Fig.13.a). Similarly, while drawing
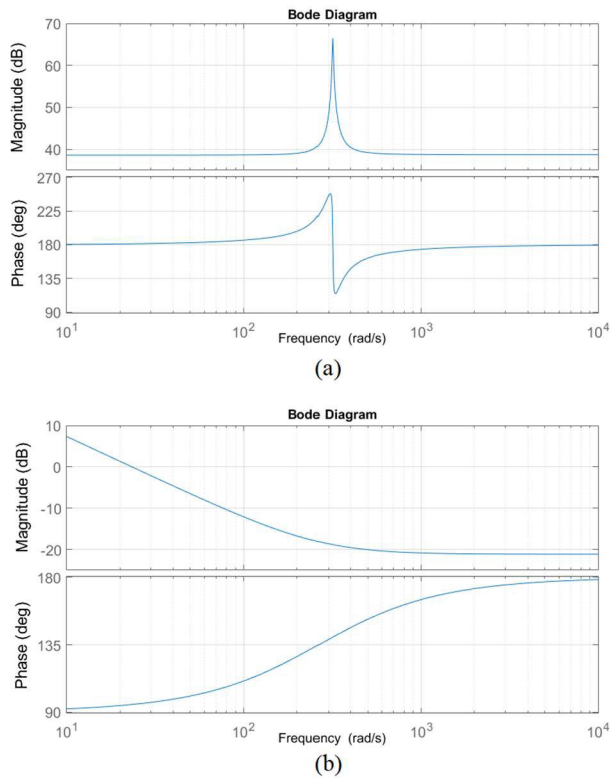
FIGURE 14. Closed-loop bode diagram (a) PR-PNN, (b) PI-PNN.

FIGURE 15. Photograph of the experimental setup.

the Vbeta_ref output graph, the inputs in the α-axis were taken as zero. The β-axis current error and the previous value were changed within the range of ± 1 A, and the graphs in Fig.13.b were created using the values of -1, -0.5, $+0.5$, and $+1$ for Vbeta_ref (k$-$1).

The PI-PNN method works in dq-axes and has three inputs for each axis: current error, the previous value of current error, and the previous value of output reference voltage. The graph of the d-axis reference voltage output control surface graphs is given in Fig.13.c. Here, the graph was prepared by taking the q-axis inputs as zero, the d-axis current error and the previous value in the range of ± 1 A, and the Vd_ref(k-1) value as fixed values (-1, -0.5, $+0.5$ and $+1$). With the same method, the surface graph of the q-axis was obtained and presented in Fig.13.d. The most critical point in these graphs is the relatively high nonlinearity of the control operation performed with the layered structure (object) and multi-surface due to the many inputs of these controllers. In addition, the closed-loop bode diagram obtained for the PR-PNN method is given in Fig.14.a, and the closed-loop bode diagram obtained for the PI-PNN method is shown in Fig.14.b. The controllers' bode diagrams were obtained using the "Bode Plot" block in Matlab/Simulink libraries. When Fig.14 is examined, it is seen that the responses of the predictive ANN controllers are similar to the responses of the controllers (PI and PR) from which the data is obtained.
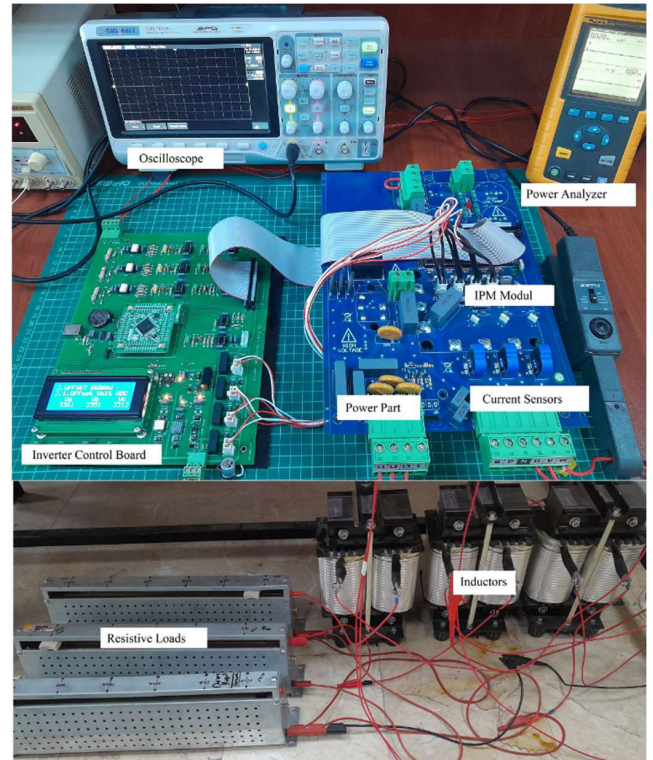
B. EXPERIMENTAL SETUP AND RESULTS

To carry out laboratory tests of the proposed models, a 5kVA three-phase inverter circuit was designed, and the photograph of its assembly is given in Fig.15. 7MBP50RJ120 1200V 50A IPM module is used in the power stage of the inverter. The current measurement is carried out with the LEM LA55-P hall effect sensor. On the inverter control card, there is a DC-DC converter circuit with four isolated 15V outputs feeding the power stage. Moreover, the control card has an LCD, control buttons, USB communication ports, a microcontroller, and signal conditioning circuits for current-voltage measurements. In the inverter control card, there is a 168 Mhz frequency STM32F407VGT6 ARM microcontroller of ST company as the microcontroller. The source code for the inverter was prepared using the MikroC for ARM compiler. As a result of the software development studies, the execution times of the algorithms were 32 μs for the MPC-ANN method, 11.6 μs for the Hist-PNN method, 10.2 μs for the PR-PNN method, and 15 μs for the PI-PNN method. In the experiments, a regulated DC source was created with a rectifier fed by the variac to which the three-phase ac grid is connected. This source was connected to the DC bus of the inverter.
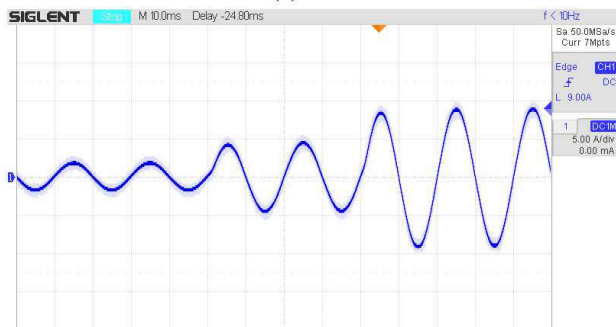
The oscilloscope images obtained from the experimental setup for MPC-ANN, Hist-PNN, PR-PNN and PI-PNN current controllers are given in Figure 16. In the study, the current reference was started as 2A and then increased to 5A and 10A, respectively. Here, the amplitude is set to 5A/div, and the time is set to 10ms/div in the oscilloscope images.
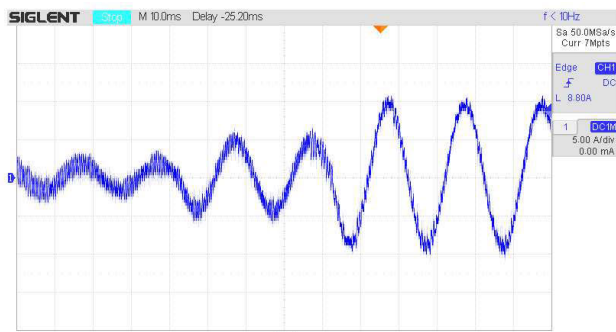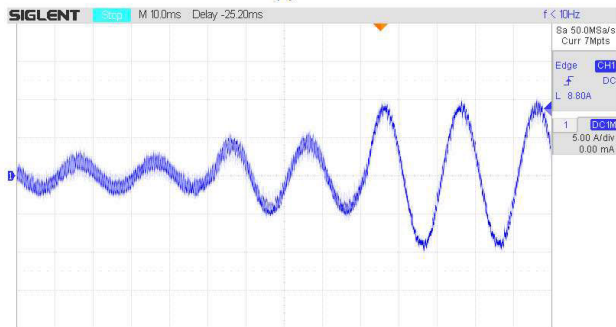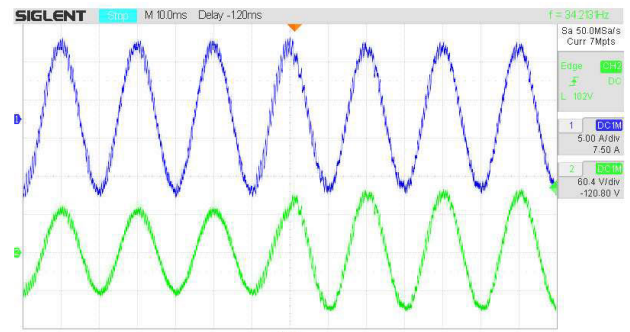
FIGURE 16. Oscilloscope images of the reference current change experiments; for (a) MPC-ANN, (b) Hist-PNN, (c) PR-PNN, and (d) PI-PNN.

FIGURE 17. Oscilloscope images of the load change experiments; for (a) MPC-ANN, (b) Hist-PNN, (c) PR-PNN, and (d) PI-PNN.

The experimental result of the MPC-ANN and Hist-PNN methods presented in Fig.16.a and 16.b contains noise at low reference currents, as seen in the simulation results. The most important reason for this is that the method's output is direct switching states. To obtain a good performance in this current controller type (MPC, Hysteresis, MPC-ANN, Hist-PNN, etc.), the operating frequencies

should be around 60-80kHz. This can increase the processing burden considerably and requires higher-performance processors. Although the MPC-ANN method is trained for different system parameters, it does not lose performance and is not affected by parameter changes.

Experimental results for the proposed PR-PNN and PI-PNN methods are given in Fig.16.c and 16.d. Both current controllers successfully follow the reference current

with low harmonic content. In addition, with the predictive feature added to their structures, the reference current was successfully followed without delay. In the training phase of these two methods, constant controller gain values and different system parameters were used. In addition, although there were noises originating from measurement units in experimental studies, they performed similarly to simulation studies. Among the important reasons for this is the ANN structure and training of data by adding random noise.

In experimental studies, THD measurements were performed using the FLUKE 43B power quality analyzer. In the measurements, total harmonic distortion (THD) for FCS-MPC CC is 3.5%, and THD for MPC-ANN CC is 3.7%. The THD for Hysteresis CC is 4.8%, and the THD for Hist-PNN CC is 2.9%. The THD value measured from the PR-PNN CC application is 1.3%. THD for classic PI CC is 1.7%, and THD for PI-PNN CC is 1.1%.

Among all the methods examined, the best performance (the lowest THD) is provided by PI-PNN CC. High non-linearity provided by the multi-layered control surface, high noise performance thanks to the dynamic ANN structure, and gained predictive ability are the most important advantages of PI-PNN CC.

In addition, the response of the designed current controllers to the load change during operation has been tested. In the experiment, 20 Ω resistors are connected in parallel to three phase 10 Ω resistive loads. The loads of 20 Ω are disabled while the inverter is working at the steady state under 10A constant reference current. Oscilloscope images were recorded for the load currents and voltages obtained during the load change and are given in Fig.17. Here, channel 1 (blue) shows the load current and channel 2 (green) shows the load voltage on the oscilloscope screen. It has been observed that the proposed current controllers adapt immediately to the new load in case of load change and successfully follow the reference current.

V. CONCLUSION

In this study, predictive current controllers are studied, and new ANN-based current controllers in four different structures are designed. In the first developed method, a network training defined as MPC-ANN CC was done with the data from the inverter system containing FCS-MPC CC. As MPC-ANN current controller, it is provided to operate at different loads without setting any parameters.

With the developed Hist-PNN, PR-PNN, and PI-PNN structures, predictive capability has been gained to classical current controllers. The ability of the developed current controllers to produce flexible outputs and to have a multi-layered control surface enables them to control non-linear systems effectively, increase their efficiency against load and parameter changes, and improve noise performance. These four different predictive ANN structures are simulated and experimentally tested under different test conditions. It has been seen that all methods have predictive properties and can be applied successfully.

REFERENCES

[1] C.-H. Lu, "Design and application of stable predictive controller using recurrent wavelet neural networks," *IEEE Trans. Ind. Electron.*, vol. 56, no. 9, pp. 3733–3742, Sep. 2009, doi: 10.1109/TIE.2009.2025714.

[2] S. S. Ge, C. Yang, and T. H. Lee, "Adaptive predictive control using neural network for a class of pure-feedback systems in discrete time," *IEEE Trans. Neural Netw.*, vol. 19, no. 9, pp. 1599–1614, Sep. 2008, doi: 10.1109/TNN.2008.2000446.

[3] B. Karanayil and M. F. Rahman, "Artificial neural network applications in power electronics and electrical drives," in *Power Electronics Handbook*. Oxford, U.K.: Butterworth-Heinemann, 2011, pp. 1139–1154, doi: 10.1016/B978-0-12-382036-5.00038-0.

[4] I. S. Mohamed, S. Rovetta, T. D. Do, T. Dragicevic, and A. A. Z. Diab, "A neural-network-based model predictive control of three-phase inverter with an output *LC* filter," *IEEE Access*, vol. 7, pp. 124737–124749, 2019, doi: 10.1109/ACCESS.2019.2938220.

[5] H. S. Khan, I. S. Mohamed, K. Kauhaniemi, and L. Liu, "Artificial neural network-based voltage control of DC/DC converter for DC microgrid applications," in *Proc. 6th IEEE Workshop Electron. Grid (eGRID)*, Nov. 2021, pp. 1–6, doi: 10.1109/eGRID52793.2021.9662132.

[6] S. Vanti, P. R. Bana, S. D'Arco, and M. Amin, "Single-stage grid-connected PV system with finite control set model predictive control and an improved maximum power point tracking," *IEEE Trans. Sustain. Energy*, vol. 13, no. 2, pp. 791–802, Apr. 2022, doi: 10.1109/TSTE.2021.3132057.

[7] D. Wang, "Model predictive control using artificial neural network for power converters," *IEEE Trans. Ind. Electron.*, vol. 69, no. 4, pp. 3689–3699, Apr. 2022, doi: 10.1109/TIE.2021.3076721.

[8] S. Borreggine, V. G. Monopoli, G. Rizzello, D. Naso, F. Cupertino, and R. Consoletti, "A review on model predictive control and its applications in power electronics," in *Proc. AEIT Int. Conf. Electr. Electron. Technol. Automot. (AEIT AUTOMOTIVE)*, Jul. 2019, pp. 1–6, doi: 10.23919/EETA.2019.8804594.

[9] J. H. Lee, "Model predictive control: Review of the three decades of development," *Int. J. Control, Autom. Syst.*, vol. 9, no. 3, pp. 415–424, Jun. 2011, doi: 10.1007/s12555-011-0300-6.

[10] S. Vazquez, J. Rodriguez, M. Rivera, L. G. Franquelo, and M. Norambuena, "Model predictive control for power converters and drives: Advances and trends," *IEEE Trans. Ind. Electron.*, vol. 64, no. 2, pp. 935–947, Feb. 2017, doi: 10.1109/TIE.2016.2625238.

[11] J. Hu, Y. Shan, J. M. Guerrero, A. Ioinovici, K. W. Chan, and J. Rodriguez, "Model predictive control of microgrids—An overview," *Renew. Sustain. Energy Rev.*, vol. 136, Feb. 2021, Art. no. 110422, doi: 10.1016/j.rser.2020.110422.

[12] V. Yaramasu, M. Rivera, M. Narimani, B. Wu, and J. Rodriguez, "Model predictive approach for a simple and effective load voltage control of four-leg inverter with an output LC filter," *IEEE Trans. Ind. Electron.*, vol. 61, no. 10, pp. 5259–5270, Oct. 2014, doi: 10.1109/TIE.2013.2297291.

[13] S. Vazquez, "Model predictive control: A review of its applications in power electronics," *IEEE Ind. Electron. Mag.*, vol. 8, no. 1, pp. 16–31, Mar. 2014, doi: 10.1109/MIE.2013.2290138.

[14] Y. Zhang and H. Lin, "Simplified model predictive current control method of voltage-source inverter," in *Proc. 8th Int. Conf. Power Electron. ECCE Asia*, May 2011, pp. 1726–1733, doi: 10.1109/ICPE.2011.5944459.

[15] J. Rodríguez, "State of the art of finite control set model predictive control in power electronics," *IEEE Trans. Ind. Informat.*, vol. 9, no. 2, pp. 1003–1016, May 2013, doi: 10.1109/TII.2012.2221469.

[16] A. Linder, R. Kanchan, R. Kennel, and P. Stolze, *Model-Based Predictive Control of Electric Drives*. Gottingen, Germany: Cuvillier Verlag, 2010.

[17] D. S. Sarali, V. A. I. Selvi, and K. Pandiyan, "An improved design for neural-network-based model predictive control of three-phase inverters," in *Proc. IEEE Int. Conf. Clean Energy Energy Efficient Electron. Circuit Sustain. Develop. (INCCES)*, Dec. 2019, pp. 1–5, doi: 10.1109/INCCES47820.2019.9167697.

[18] O. Machado, P. Martín, F. J. Rodríguez, and E. J. Bueno, "A neural network-based dynamic cost function for the implementation of a predictive current controller," *IEEE Trans. Ind. Informat.*, vol. 13, no. 6, pp. 2946–2955, Dec. 2017, doi: 10.1109/TII.2017.2691461.

[19] A. A. S. Mohamed, H. Metwally, A. El-Sayed, and S. I. Selem, "Predictive neural network based adaptive controller for grid-connected PV systems supplying pulse-load," *Sol. Energy*, vol. 193, pp. 139–147, Nov. 2019, doi: 10.1016/j.solener.2019.09.018.

[20] A. Bakeer, I. S. Mohamed, P. B. Malidarreh, I. Hattabi, and L. Liu, "An artificial neural network-based model predictive control for three-phase flying capacitor multilevel inverter," *IEEE Access*, vol. 10, pp. 70305–70316, 2022, doi: 10.1109/ACCESS.2022.3187996.

[21] M. Novak and T. Dragicevic, "Supervised imitation learning of finite-set model predictive control systems for power electronics," *IEEE Trans. Ind. Electron.*, vol. 68, no. 2, pp. 1717–1723, Feb. 2021, doi: 10.1109/TIE.2020.2969116.

[22] P. R. Bana and M. Amin, "Comparative assessment of supervised learning ANN controllers for grid-connected VSC system," in *Proc. IECON 48th Annu. Conf. IEEE Ind. Electron. Soc.*, Oct. 2022, pp. 1–6, doi: 10.1109/IECON49645.2022.9969070.

[23] E. G. Oxnevad, *Artificial Neural Network-Based Control for Grid-Connected Converter*. Trondheim, Norway: Norwegian University of Science and Technology, 2022. [Online]. Available: https://ntnuopen.ntnu.no/ntnu-xmlui/handle/11250/3023810?show=full

[24] M. Semasa, T. Kato, and K. Inoue, "Simple and effective time delay compensation method for active damping control of grid-connected inverter with an LCL filter," *IEEJ J. Ind. Appl.*, vol. 7, no. 6, pp. 454–461, Nov. 2018, doi: 10.1541/ieejjia.7.454.

[25] G. Mirzaeva and G. C. Goodwin, "Harmonic suppression and delay compensation for inverters via variable horizon nonlinear model predictive control," *Int. J. Control*, vol. 88, no. 7, pp. 1400–1409, Jul. 2015, doi: 10.1080/00207179.2014.948915.

[26] J. I. Leon, S. Kouro, L. G. Franquelo, J. Rodriguez, and B. Wu, "The essential role and the continuous evolution of modulation techniques for voltage-source inverters in the past, present, and future power electronics," *IEEE Trans. Ind. Electron.*, vol. 63, no. 5, pp. 2688–2701, May 2016, doi: 10.1109/TIE.2016.2519321.

[27] M. Rivera, F. Morales, C. Baier, J. Munoz, L. Tarisciotti, P. Zanchetta, and P. Wheeler, "A modulated model predictive control scheme for a two-level voltage source inverter," in *Proc. IEEE Int. Conf. Ind. Technol. (ICIT)*, Mar. 2015, pp. 2224–2229, doi: 10.1109/ICIT.2015.7125425.

[28] Y. Yang, H. Wen, and D. Li, "A fast and fixed switching frequency model predictive control with delay compensation for three-phase inverters," *IEEE Access*, vol. 5, pp. 17904–17913, 2017, doi: 10.1109/ACCESS.2017.2751619.

[29] Z. Song, Y. Tian, W. Chen, Z. Zou, and Z. Chen, "Predictive duty cycle control of three-phase active-front-end rectifiers," *IEEE Trans. Power Electron.*, vol. 31, no. 1, pp. 698–710, Jan. 2016, doi: 10.1109/TPEL.2015.2398872.

[30] P. Cortes, S. Kouro, B. L. Rocca, R. Vargas, J. Rodriguez, J. I. Leon, S. Vazquez, and L. G. Franquelo, "Guidelines for weighting factors design in model predictive control of power converters and drives," in *Proc. IEEE Int. Conf. Ind. Technol.*, Feb. 2009, pp. 1–7, doi: 10.1109/ICIT.2009.4939742.

SÜLEYMAN YARIKKAYA received the B.Sc. degree in electronic engineering from Erciyes University, Kayseri, in 2003, and the M.Sc. degree in electrical engineering (renewable energy systems) from Afyon Kocatepe University, Afyon, in 2015. He is currently pursuing the Ph.D. degree with Kütahya Dumlupınar University, Kütahya, Turkey.

Since 2012, he has been working as a Lecturer at the Afyon Kocatepe University, Dinar Vocational School, Department of Computer Programming. His research interests include the control of power converters, renewable energy, model predictive control, artificial intelligence, and programming for embedded systems.

KADİR VARDAR (Member, IEEE) received the B.Sc. and M.Sc. degrees in electrical and electronics engineering from Kütahya Dumlupınar University, Turkey, in 2001 and 2004, respectively, and the Ph.D. degree in electrical and electronics engineering from Dokuz Eylul University, in 2011.

He is currently an Assistant Professor with the Department of Electrical and Electronics Engineering, Kütahya Dumlupınar University. His research interests include power electronics, inverters, motor drives, and embedded systems.

● ● ●